

Parameter Estimation with Dense and Convolutional Neural Networks Applied to the FitzHugh–Nagumo ODE

Johann Rudi^{*†}

Julie Bessac^{*}

Amanda Lenzi^{*}

December 22, 2024

Abstract

Machine learning algorithms have been successfully used to approximate nonlinear maps under weak assumptions on the structure and properties of the maps. We present deep neural networks using dense and convolutional layers to solve an inverse problem, where we seek to estimate parameters in a FitzHugh–Nagumo model, which consists of a nonlinear system of ordinary differential equations (ODEs). We employ the neural networks to approximate reconstruction maps for model parameter estimation from observational data, where the data comes from the solution of the ODE and takes the form of a time series representing dynamically spiking membrane potential of a (biological) neuron. We target this dynamical model because of the computational challenges it poses in an inference setting, namely, having a highly nonlinear and nonconvex data misfit term and permitting only weakly informative priors on parameters. These challenges cause traditional optimization to fail and alternative algorithms to exhibit large computational costs. We quantify the predictability of model parameters obtained from the neural networks with statistical metrics and investigate the effects of network architectures and presence of noise in observational data. Our results demonstrate that deep neural networks are capable of very accurately estimating parameters in dynamical models from observational data.

1 Introduction

We consider inverse problems with the aim of estimating parameters from given observational data, where the parameters give rise to the data through the solution of a parameterized physical model. Such inverse problems have in the past been solved deterministically with techniques from optimization [42] or in a statistical/Bayesian framework using sampling methods, particle filters, and Kalman filters [27]. The current work investigates new approaches to solving particular inverse problems that exhibit computational challenges prohibiting effective use of the established solution techniques mentioned above. We propose to computationally learn solution operators for inverse problems based on deep neural networks because of their well-known potential of finding generalizable nonlinear maps. We explore neural network (NN) architectures consisting of a sequence of dense, or fully connected, layers and convolutional neural networks (CNNs).

We target inverse problems to estimate parameters in an ordinary differential equation (ODE) that models the dynamically spiking membrane potential of a (biological) neuron. Spiking neurons in the brain and spinal cord are typically modeled by systems of nonlinear ODEs. These ODE models govern electrical voltage spikes that are generated in response to current stimuli. The

^{*}Mathematics and Computer Science Division, Argonne National Laboratory, Lemont IL, USA

[†]jrudi@anl.gov

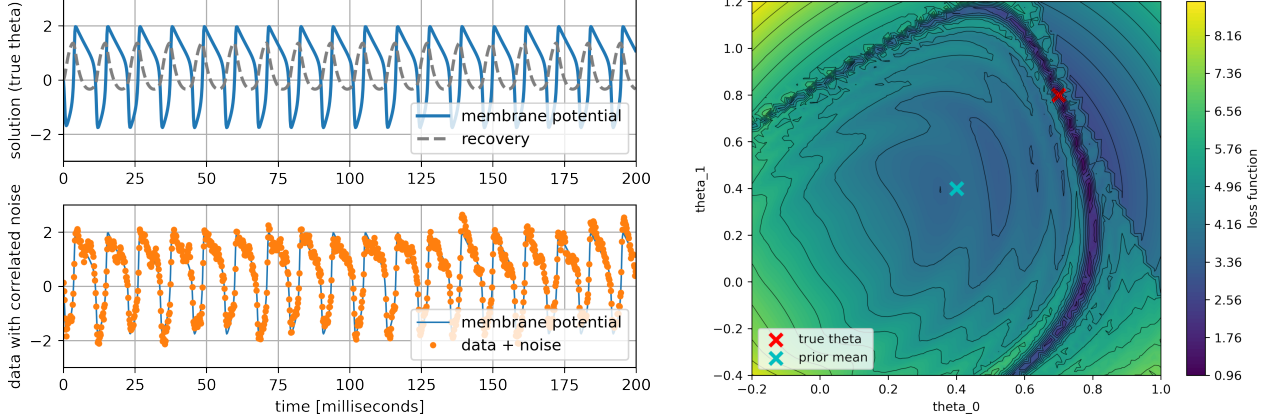


Figure 1: Top left graph: Solution of FitzHugh–Nagumo system of two ODEs (blue and gray lines) generated with true parameters of the inverse problem. Bottom left graph: Data (orange dots) of inverse problem stemming from the membrane potential of the solution with additive correlated noise. Right: Manifold of highly nonlinear loss function (colors and contours), with respect to parameters θ_0 and θ_1 , of the inverse problem governed by the FitzHugh–Nagumo model when using the data from the bottom left graph and a weakly informative (i.e., wide) prior term.

output of one such ODE has the form of a spiking voltage time series, which can be obtained in laboratory experiments and takes the role of observational data in our inverse problem. These systems of ODEs contain uncertain parameters that control the opening and closing of ion channels of a cell membrane and consequently change voltage spike behavior.

Computational challenges arise from the highly nonlinear and nonconvex loss, or objective, function of the inverse problem ([6]; see also the manifold in Figure 1, right), with sharp gradients, strong nonlinear dependencies between parameters, and potentially multiple local minima. The loss cannot be sufficiently regularized by a convex additive term stemming from a regularization or prior term, because of lack of knowledge about the range of parameter values [21, 38] and because this would largely eliminate the information from data and model. We therefore explore new techniques to solve such challenging inverse problems by fitting NN-based reconstruction maps that approximate solution operators for our inverse problem by means of mapping observational data to model parameters.

Contributions We consider neural networks with dense and convolutional layers and explore different NN architectures with a range of layers, dense units, and CNN filters. We quantify the capability of the networks to approximate reconstruction maps of inverse problems with several statistical metrics. Through these metrics, we aim to provide understanding about the effects of network choice on inference performance. The numerical results show that NNs can estimate parameters of spiking neuron models with high accuracy. We additionally investigate the predictability of model parameters by NNs while changing the sizes of training sets. Moreover, because observational data are in practice most likely corrupted by noise and because we believe the effects of noise have not been sufficiently addressed in the literature for the inference we are attempting, we present a noise model and analyze the influence of noise in training and/or testing data.

Related work The literature on parameter estimation for models of neural dynamics spans across various scientific communities, approaches, and neuron models. Here, we highlight only closely

related publications and refer to the literature within these publications for further information. The neuron model by [24] is often used in the literature. It consists of a nonlinear system of four ODEs. The FitzHugh–Nagumo equations (introduced in Section 2.1) simplify the Hodgkin–Huxley model to a nonlinear system of two ODEs.

Common approaches for parameter estimation in FitzHugh–Nagumo and Hodgkin–Huxley models make use of heuristics and trial and error and may consist of intricate sequences of regression steps, as summarized by [6] and [44]. The techniques employed are, for instance, simulated annealing, differential evolution, genetic algorithms, and brute-force grid search [3]. These approaches have the disadvantage of being computationally expensive or slow to converge. Using gradient descent for finding the minimizer of a Hodgkin–Huxley-based inverse problem [14], on the other hand, suffers from the strong nonlinearities in the objective and requires good initial guesses. Alternative approaches estimate parameters with maximum likelihood methods and build approximations of the likelihood term [15]. Recently, Kalman filters have been utilized, for instance, by [13]; ensemble Kalman filters are combined with reduced order models [36], and augmented ensemble Kalman filters [4] are employed for periodically time-varying parameters. In a data assimilation framework, [22] propose an ensemble Kalman filter for time series with large amounts of noise. Furthermore, statistical inference in a Bayesian framework is attempted with approximate Bayesian computation (ABC) [11] and Monte Carlo sampling [12]. Alternatively to time series data, [26] and [34] develop inference methods for spike time data.

While machine learning techniques generally are used for prediction and classification tasks in a wide range of applications, they are employed more sparsely to estimate parameters of mathematical models. For instance, [32] (for groundwater modeling) and [16] (for kinetic models) utilize NNs within their parameter estimation frameworks for systems described by partial or ordinary differential equations, they however do not consider approximating reconstruction maps. [37] employ generative adversarial networks to retrieve model parameters in stochastic inverse problems. Parameter estimation approaches for neural dynamics based on NNs are proposed [19], where an NN is trained to perform posterior density estimates using mixtures of Gaussian or normalizing flows. While [19] show promising approximations of posterior features, their approach comes at the cost of large training sets (of order 10^5), which is about two orders of magnitude larger than in our work. Each training sample requires the solution of an ODE model and, if performed frequently, constitutes the major computational cost. For such large numbers of training samples, Monte Carlo methods [5] become preferable alternatives, especially if they could be augmented with reduced order models [39, 35]. Moreover, [19] do not analyze the effects of noise in training and/or testing data, and training set sizes are not varied. Their network architectures are prescribed, which reflects an inductive bias [9] by knowing which network performs well for a given problem.

In statistical models, machine learning is used for direct estimation of model parameters [7], where NNs are used for estimating autoregressive moving-average processes parameters. [40] propose a suite of two NNs to estimate summary statistics of the data, infer parameters of a model, and return samples from the posterior distributions. Other works focus on supplementing or complementing statistical inferential techniques with machine learning. In particular, problems with intractable likelihood are often solved with the ABC method involving the sampling of synthetic data and summary statistics of the observations. [10] and [25] uses an NN to predict the parameters from artificially generated data, which are then used as an estimate of the posterior mean of an ABC procedure.

The remainder of the paper is organized as follows. Section 2 begins with the forward problem governed by the FitzHugh–Nagumo model and the corresponding inverse problem in order to estimate parameters of the model. It then presents NN architectures utilized for solving the

inverse problem, the generation of training and testing samples, and metrics to evaluate NN-based model parameter estimates. Section 3 discusses numerical results and quantifies the predictability of model parameters from trained NNs. We consider a range of network architectures, different sizes of training data, and the effects of noise. Section 4 presents conclusive remarks and remaining open questions.

2 Neural network-based reconstruction maps for inverse problems

This section introduces the forward problem that is governed by the FitzHugh–Nagumo ODE and the inverse problem to estimate model parameters of the ODE from time series data. Furthermore, we describe the NN architectures that will be used to perform the inference. We conclude this section with a set of metrics that we use to evaluate the errors of model parameter predictions coming from the NNs.

2.1 Forward and inverse modeling of spiking neurons

The FitzHugh–Nagumo [18, 33] equations describe spiking neurons via a system of two ODEs,

$$\frac{du}{dt} = \gamma \left(u - \frac{u^3}{3} + v + \zeta \right), \quad (1a)$$

$$\frac{dv}{dt} = -\frac{1}{\gamma} (u - \theta_0 + \theta_1 v), \quad (1b)$$

where the unknowns of the ODE are the membrane potential $u = u(t)$ and the recovery variable $v = v(t)$. ζ denotes the total membrane current and is a stimulus applied to the neuron, which we assume to be constant in time. γ is constant, and θ_0 and θ_1 are the model parameters that will be considered for inference below. The ODE (1) is augmented with initial conditions $u(0) = u_0$ and $v(0) = v_0$. An example solution of (1) is shown in the top left panel of Figure 1, using $\theta_0 = 0.7$, $\theta_1 = 0.8$, $\gamma = 3.0$, $\zeta = -0.4$, and $u_0 = v_0 = 0$. While the FitzHugh–Nagumo model formulation is relatively simple compared with larger systems of ODEs, like the Hodgkin–Huxley equations, it exhibits most of the computational challenges when considered as the forward problem in an inference setting, such as described next.

We target the inverse problem, where we are given observational data

$$d(t) := u_{\theta^*}(t) + \eta(t) \quad (2)$$

composed of the first component $u_{\theta^*}(t)$ of the solution of (1) with (unknown) true parameters $\theta^* := (\theta_0^*, \theta_1^*)$ and added correlated noise $\eta(t)$ (see Section 3.3 for more information about the noise model). Our goal is to find parameters $\theta := (\theta_0, \theta_1)$ that are consistent with data $d(t)$ and model output $u_{\theta}(t)$ for all t . Note that the second variable v of the ODE (1) is excluded from the data because typically only the membrane potential can be observed in experiments. In a statistical/Bayesian framework [27], the inverse problem translates to finding the posterior probability density $\pi(\theta | d)$ of the parameters θ given data d , where d is a discretization of $d(t)$. The posterior is, via Bayes' rule, composed of a likelihood term $\pi(d | \theta)$ and a prior term $\pi(\theta)$,

$$\pi(\theta | d) \propto \pi(d | \theta) \pi(\theta). \quad (3)$$

Our prior on the parameters θ is chosen to be only weakly informative (i.e., relatively large variance), because we assume little knowledge about the distribution of θ . Since in practice parameters

of the FitzHugh–Nagumo model are chosen such that $\theta_0, \theta_1 \in [0, 1]$, our prior specifies that each parameter is normal and i.i.d. (independent identically distributed),

$$\theta_0 \sim \mathcal{N}(0.4, 0.3) \quad \text{and} \quad \theta_1 \sim \mathcal{N}(0.4, 0.4). \quad (4)$$

Additionally, we limit the range of parameters to be inside the intervals

$$\theta_0 \in [-0.2, 1.0] \quad \text{and} \quad \theta_1 \in [-0.4, 1.2] \quad (5)$$

by means of rejecting prior samples outside of these bounds. Note that these parameter bounds reflect our prior knowledge for the inverse problem and are not required for solvability of the FitzHugh–Nagumo equations (1). The resulting highly nonlinear loss function of our inverse problem is shown in Figure 1, right, where we used the squared L_2 -norm, $\|d - u_{\theta}\|_{L_2}^2$, for the data misfit term. As discussed in the introduction, this loss function presents significant challenges for computational solution techniques.

In the following, we construct NNs to infer point estimates of θ from a given time series d . A similar point estimate of the posterior density (3), called the maximum a posteriori (MAP) point, can be obtained by minimizing the negative log of (3),

$$\hat{\theta}_{\text{MAP}} = \arg \min_{\theta} \left[-\log(\pi(d | \theta) \pi(\theta)) \right]. \quad (6)$$

Hence our NN-based reconstruction maps aim for approximating solutions of (6).

2.2 Deep neural networks for inverse problems

We construct NNs to computationally learn reconstruction maps of the inverse problem (6). We set up the training data such that the inputs of the NN are time series (2) coming from the solution of the ODE (1) and the outputs are the corresponding parameters θ that generated the time series. Since we train the NN to fit a mapping of time series to parameters in the reverse order of the forward problem, the NN is learning to represent a pseudoinverse of the forward operator, as defined by [1], hence approximately solving an inverse problem. We define our NN-based reconstruction map as

$$\hat{\theta} := y_L, \quad y_{\ell} = \mathcal{F}_{\ell}(y_{\ell-1}) \text{ for } 1 \leq \ell \leq L, \quad y_0 := d, \quad (7)$$

where NN input d is a discrete version of the time series (2), \mathcal{F}_{ℓ} denotes layer ℓ of the NN, and $\hat{\theta}$ is the network's output, which are predicted model parameters. We regard the NN's prediction of model parameters $\hat{\theta}$ as analogous to point estimates, such as solutions of (6).

Training and testing data for neural networks We generate training and testing data for NNs by sampling parameters θ from their prior distributions (4) and discarding samples outside of prior bounds (5). By choosing samples from the prior to generate training data, we want the NN reconstruction (7) to learn the most important features of our inverse problem according to prior knowledge. By using prior samples for training, we additionally try to achieve a correspondence between the original inverse problem (6) and our NN reconstruction maps (7). Having obtained samples of θ , we solve the ODE (1) and store the membrane potential $u_{\theta}(t_i)$ at prescribed time steps, t_i , $i = 1, \dots, N_t$, with uniform step size Δ_t . The next two paragraphs describe the different architectures for the layers denoted by \mathcal{F}_{ℓ} in Equation (7).

Dense neural network (dense NN) Our first NN architectures consist of a sequence of dense, or fully connected, layers [20]. Each dense layer consists of n_u units, or nodes, and each unit of one layer is connected to all other units of a neighboring layer. One dense layer is written as a composition of affine mapping and nonlinear function,

$$\mathcal{F}_\ell(y_{\ell-1}) = \phi(W_\ell y_{\ell-1} + b_\ell), \quad (8)$$

where matrix $W_\ell \in \mathbb{R}^{n_u \times n_u}$ is called the weights and $b_\ell \in \mathbb{R}^{n_u}$ the bias of layer ℓ . The nonlinear activation function ϕ is applied element-wise. A typical choice for ϕ is the rectified linear unit (ReLU) function [41]. We, however, utilize a smoother activation similar to ReLU, called Swish [17]. NNs with Swish activation have been shown to suffer less from vanishing gradient problems compared with ReLU [23], and this behavior has been also observed by the authors when training deeper networks. For our numerical experiments in Section 3, we use dense NNs with 2–16 layers and 4–128 units n_u in all layers to cover a wide range of network sizes, which we will demonstrate to be sufficient for accurate approximation of reconstruction maps. The dense NNs amount to a total of between 4,034 and 442,114 NN parameters in the form of weight matrices W_ℓ and biases b_ℓ , which are optimized with stochastic gradient descent by using the Adam algorithm [28] and the mean squared error (MSE) loss function (see Section 3.1 for more details).

Convolutional neural network (CNN) CNNs have been successfully used in two-dimensional image-processing tasks [30]. We take advantage of the local dependence structure inherent in CNNs to fit reconstruction maps (7) that have one-dimensional time series with uniform time steps as input. We therefore exploit locality in our time series with convolutional layers. A convolutional layer is composed of n_f filters, and each filter is associated with one kernel that is applied to small sections of the time series. The n_f kernels of one convolutional layer are connected to all neighboring layers, similarly to the units of dense layers described above. The weights of these connections constitute the NN parameters to be optimized. Because the weights are shared across time, significantly fewer weights have to be optimized.

Our convolutional architectures borrow from CNNs for image classification [29], where we interleave convolutional layers with pooling layers (also called downsampling), which aggregate a small block from a convolutional step into a single value. Each convolutional layer, $y_\ell = \mathcal{F}_\ell(y_{\ell-1})$, reduces the size of output vectors y_ℓ compared with input $y_{\ell-1}$, here by a factor of 1/2; the same reduction holds for pooling layers. The reduction in size is complemented with an increase of n_f filter counts, here by a factor of 2, from one convolutional layer to the next. After a few combinations of convolution and pooling, the output is passed to a sequence of dense layers, which concludes the CNN. Our CNNs are equipped with 2–4 pairs of convolution and pooling layers with varying numbers of filters (see Section 3.2 for more details), and we keep the dense layers at the end of the network fixed to two layers with $n_u = 32$ units. These CNNs achieve NN parameter counts between 5,278 and 261,442. We utilize the same Swish activation function and optimization setup as for dense NNs described above.

2.3 Evaluation metrics for inference results

To assess the quality of the prediction from NNs, we carry out both qualitative and quantitative evaluations in Section 3. Qualitative assessments are done through scatter plots and time series plots, and the quantification of predictability is evaluated with several metrics.

In particular, we decompose the commonly used mean squared error (MSE) into its squared bias and centered MSE (C-MSE) components to assess the respective contributions of the mean

and of the fluctuations (variability) of the prediction mismatch [43]:

$$\text{MSE}(\boldsymbol{\theta}, \hat{\boldsymbol{\theta}}) := \frac{1}{M} \sum_{j=1}^M \left(\boldsymbol{\theta}^{(j)} - \hat{\boldsymbol{\theta}}^{(j)} \right)^2 = \underbrace{\left(\bar{\boldsymbol{\theta}} - \hat{\bar{\boldsymbol{\theta}}} \right)^2}_{=: \text{Squared bias}} + \underbrace{\frac{1}{M} \sum_{j=1}^M \left[\left(\boldsymbol{\theta}^{(j)} - \bar{\boldsymbol{\theta}} \right) - \left(\hat{\boldsymbol{\theta}}^{(j)} - \hat{\bar{\boldsymbol{\theta}}} \right) \right]^2}_{=: \text{C-MSE}},$$

where $\boldsymbol{\theta}$ is the true model parameter, $\hat{\boldsymbol{\theta}}$ is the predicted parameter, $\bar{\boldsymbol{\theta}}$ (resp. $\hat{\bar{\boldsymbol{\theta}}}$) is the mean of true parameters (resp. estimated parameters), and M is the training set size. We use superscript notation (e.g., $\boldsymbol{\theta}^{(j)}$) to identify different parameters in the training set. A smaller MSE implies lower errors and hence better predictions.

Since MSE has the disadvantage of being sensitive to large errors, we report the median of the absolute percentage error (Median-APE), $|\boldsymbol{\theta}^{(j)} - \hat{\boldsymbol{\theta}}^{(j)}|/|\boldsymbol{\theta}^{(j)}|$, between true $\boldsymbol{\theta}^{(j)}$ and estimated $\hat{\boldsymbol{\theta}}^{(j)}$ model parameters. This also provides a scale-invariant metric that is less sensitive to outliers than a mean statistic is. The coefficient of determination R^2 is used to assess the percentage of variability explained by the prediction

$$R^2 = 1 - \frac{\sum_{j=1}^M \left(\boldsymbol{\theta}^{(j)} - \hat{\boldsymbol{\theta}}^{(j)} \right)^2}{\sum_{j=1}^M \left(\boldsymbol{\theta}^{(j)} - \bar{\boldsymbol{\theta}} \right)^2}.$$

The R^2 takes values between $-\infty$ and 1; the closer to 1, the more variability is explained by the prediction, and hence observed outcomes are better replicated by the model.

3 Numerical experiments

In this section we analyze the accuracy of model parameter estimates from dense NNs and CNNs defined in Section 2.2. We first investigate the effects of different network architectures on the predictability of FitzHugh–Nagumo model parameters, and we subsequently analyze the sensitivity of predictions in the presence of noise in training and/or testing data. For these analyses, we utilize the metrics described in Section 2.3. We conclude the numerical experiments by simulating the forward problem with predicted parameters to assess the correspondence of observational data with model outputs arising from predictions.

3.1 Experimental setup

The implementation of our algorithms is carried out in Python. We use the explicit Runge–Kutta method of order 3(2) (RK23) for time integration of the FitzHugh–Nagumo ODE, and we utilize TensorFlow/Keras (version 2.3.1) for implementing the neural networks. To generate training and testing data for the networks, we simulate the FitzHugh–Nagumo ODE (1) for 200 milliseconds and store the membrane potential at equidistant steps every $\Delta_t = 0.2$, which results in a time series of size $N_t = 1000$ for each model parameter $\boldsymbol{\theta}$. We use $N = 1000$ random training samples unless otherwise specified, and we fix $M = 2000$ randomly chosen testing samples throughout all experiments in order to fairly evaluate the parameter estimates provided by different networks and experimental setups. Table 1 provides a summary of the experimental settings regarding the optimizer for the neural networks, and Table 2 shows our settings for network architectures.

Table 1: Settings for training/testing data and optimization algorithms.

Training & optimization setting	Value
Number of training samples (N)	1000
Number of test samples (M)	2000
Size of time series (N_t)	1000
Loss function	MSE
Optimizer	Adam
Learning rate (or step length)	0.002
Batch size	32
Number of epochs with noise-free data	200
Number of epochs with noisy data	50

Table 2: Settings for dense and convolutional neural network architectures.

Neural network setting	Value
Activation function (dense NN & CNN)	Swish
CNN kernel size	3
CNN kernel stride	2
CNN pooling type	average
CNN pooling size	2
CNN pooling stride	2
CNN padding	none

Table 3: Squared bias (C-MSE) of model parameter predictions (noise-free), using **dense NNs** with variable numbers of layers and units per layer n_u .

n_u	2 layers	4 layers	8 layers	12 layers	16 layers
4	3.0×10^{-5} (0.0313)	9.1×10^{-5} (0.0020)	2.3×10^{-4} (0.0049)	9.8×10^{-5} (0.0211)	1.3×10^{-4} (0.0090)
8	8.7×10^{-5} (0.0035)	4.7×10^{-4} (0.0028)	3.6×10^{-5} (0.0025)	1.7×10^{-4} (0.0040)	3.2×10^{-5} (0.0051)
16	7.6×10^{-5} (0.0022)	2.2×10^{-5} (0.0020)	1.5×10^{-5} (0.0022)	8.0×10^{-5} (0.0025)	5.0×10^{-5} (0.0022)
32	6.1×10^{-5} (0.0024)	6.5×10^{-6} (0.0020)	8.7×10^{-5} (0.0019)	7.7×10^{-5} (0.0019)	1.7×10^{-4} (0.0020)
64	1.5×10^{-5} (0.0021)	1.2×10^{-4} (0.0023)	8.0×10^{-5} (0.0018)	3.0×10^{-4} (0.0017)	3.8×10^{-4} (0.0027)
128	1.1×10^{-5} (0.0024)	5.2×10^{-5} (0.0029)	4.5×10^{-4} (0.0025)	1.4×10^{-4} (0.0018)	3.5×10^{-4} (0.0027)

Table 4: Median-APE (R^2) of model parameter predictions (noise-free), using **dense NNs** with variable numbers of layers and units per layer n_u .

n_u	2 layers	4 layers	8 layers	12 layers	16 layers
4	0.116 (0.570)	0.043 (0.978)	0.061 (0.951)	0.237 (0.763)	0.094 (0.902)
8	0.052 (0.960)	0.060 (0.967)	0.048 (0.975)	0.055 (0.958)	0.041 (0.951)
16	0.034 (0.977)	0.035 (0.980)	0.026 (0.978)	0.043 (0.975)	0.030 (0.977)
32	0.034 (0.976)	0.030 (0.980)	0.027 (0.980)	0.039 (0.980)	0.030 (0.979)
64	0.027 (0.979)	0.026 (0.977)	0.033 (0.981)	0.037 (0.980)	0.053 (0.969)
128	0.024 (0.977)	0.033 (0.971)	0.045 (0.970)	0.036 (0.981)	0.072 (0.969)

3.2 Exploration of neural network architectures

In the following, we investigate the influence of different NN architectures from Section 2.2 on predictions performed on test data. The evaluation is based on the metrics defined in Section 2.3 in order to describe statistical properties of the predicted model parameters. We explore effects on predictability while varying the number of dense layers and number of units per layer, in the case of dense NNs, and the number of convolutional layers and filters per layer, in the case of CNNs. The training of the networks as well as predictions is performed on noise-free time series data, which represents an ideal scenario. Noise-free data have the advantage that optimization algorithms, using stochastic gradient descent here, can be performed for sufficiently high iteration counts (or epochs), without leading to overfitting due to noise in the data. This allows us to train the networks relatively well and therefore investigate differences in predictions that are largely due to network architectures. Prediction results with noise added to observational data are crucial in practice and are presented in Section 3.3.

Table 5: Squared bias (C-MSE) of model parameter predictions (noise-free), using **CNNs** with variable numbers of convolutional layers and filters per layer n_f .

n_f	$n_f \times [1, 2]$	$n_f \times [1, 2, 4]$	$n_f \times [1, 2, 4, 8]$
2	6.3×10^{-5} (0.000 67)	7.9×10^{-5} (0.000 55)	3.2×10^{-5} (0.000 50)
4	1.3×10^{-5} (0.001 60)	6.5×10^{-5} (0.000 52)	6.4×10^{-5} (0.000 41)
8	1.5×10^{-4} (0.001 29)	1.9×10^{-5} (0.000 38)	3.3×10^{-5} (0.000 42)
16	4.6×10^{-4} (0.001 35)	1.2×10^{-5} (0.000 65)	2.4×10^{-5} (0.000 60)
32	3.0×10^{-4} (0.001 04)	3.6×10^{-6} (0.000 57)	5.9×10^{-6} (0.000 58)

Table 6: Median-APE (R^2) of model parameter predictions (noise-free), using **CNNs** with variable numbers of convolutional layers and filters per layer n_f .

n_f	$n_f \times [1, 2]$	$n_f \times [1, 2, 4]$	$n_f \times [1, 2, 4, 8]$
2	0.025 (0.992)	0.029 (0.993)	0.017 (0.994)
4	0.021 (0.984)	0.018 (0.994)	0.024 (0.995)
8	0.032 (0.985)	0.017 (0.995)	0.021 (0.995)
16	0.042 (0.982)	0.021 (0.993)	0.031 (0.993)
32	0.032 (0.987)	0.022 (0.993)	0.022 (0.993)

Model parameter predictions with dense NNs The predictability properties of dense NNs is evaluated with the squared bias and C-MSE metrics in Table 3 for the number of dense layers varying from 2 to 16 while using between 4 and 128 units per layer, n_u . Corresponding evaluations with the Median-APE and R^2 metrics are shown in Table 4. The tables highlight in red those configurations leading to relatively poor predictions and in green those leading to relatively good predictions. Overall, we observe a low error in average squared bias (below 10^{-3}) and mild variations of the errors, expressed in C-MSE values below 10^{-2} , showing that a large contribution to the total MSE is due to the mismatch in variability between true and predicted parameters. Additionally, the scale invariant metric Median-APE assumes values mostly below 10^{-1} and the R^2 metric mostly above 0.95. From these tables, we can deduce that networks with 4–12 layers and 32–64 units per layer lead to the lowest prediction errors (green cells in Tables 3, 4). Networks with small unit counts, such as 4, however, deteriorate in their predictability, because they do not offer sufficient degrees of freedom. Furthermore, deeper networks with large numbers of layers, such as 16, do not offer any improvements in predictability compared with shallower architectures. Next, we improve upon the already good results of dense NNs by using convolutional layers.

Model parameter predictions with CNNs Analogous to the results with dense NNs, we investigate the CNN predictability while changing the number of convolutional layers and the number of filters n_f per layer. Two dense layers with 32 units follow the convolutional layers and remain fixed during these experiments. Table 5 shows evaluations with squared bias and C-MSE metrics, and Table 6 considers the Median-APE and R^2 metrics. As in the previous tables, we use red color to highlight network architectures leading to relatively poor predictions and green color to highlight relatively good predictions. We express the convolutional layers as a list, for instance $n_f \times [1, 2, 4]$, which denotes $n_f \times 1 = n_f$ filters in the first layer, $n_f \times 2 = 2n_f$ filters in the second layer, and $n_f \times 4 = 4n_f$ filters in the third layer. Tables 5 and 6 show that CNNs can further improve the predictability for our inverse problem compared with dense NNs. This improvement is demonstrated by C-MSE values below 10^{-3} (one order of magnitude lower than with dense NNs) and R^2 values mostly above 0.99 (previously 0.95–0.98 with dense NNs), which

Table 7: Median-APE (R^2) of model parameter predictions with noisy observational data, using a **dense NN** with 4 layers, $n_u = 32$.

N	train	noise-free	train	noise-free	train	with noise
	test	noise-free	test	with noise	test	with noise
500	0.047 (0.961)		0.105 (0.916)		0.126 (0.875)	
1000	0.030 (0.980)		0.099 (0.931)		0.088 (0.927)	
4000	0.025 (0.991)		0.084 (0.952)		0.060 (0.964)	
8000	0.020 (0.995)		0.090 (0.944)		0.050 (0.974)	

Table 8: Median-APE (R^2) of model parameter predictions with noisy observational data, using a **CNN** with $n_f \times [1, 2, 4]$, $n_f = 8$.

N	train	noise-free	train	noise-free	train	with noise
	test	noise-free	test	with noise	test	with noise
500	0.039 (0.989)		0.137 (0.895)		0.104 (0.920)	
1000	0.017 (0.995)		0.145 (0.880)		0.083 (0.955)	
4000	0.013 (0.998)		0.148 (0.860)		0.059 (0.971)	
8000	0.015 (0.999)		0.147 (0.870)		0.055 (0.975)	

is very close to the ideal R^2 of 1.0. These improvements relative to dense NN can be attributed to the CNNs exploiting local information of neighboring points in the time series.

We additionally observe that CNNs with only two convolutional layers yield significantly higher prediction errors than with three and four layers. Thus the short networks do not offer sufficient degrees of freedom to adapt to the reconstruction map of the inverse problem and generalize to unseen test data. Moreover, increasing the number of filters n_f to 16 and beyond (in the first layer) shows no benefit in predictability. The best results are achieved with 3–4 convolutional layers and 4–8 filters n_f (in the first layer), which we highlight by green cells in the tables.

3.3 Predictability in the presence of noise in observational data

Additive noise model We consider an additive noise model that is first-order autoregressive in time, a widely used representation of time series data parametrized by a correlation parameter ρ , which determines the dependence of the process on its previous value [31]. Recall from (2) that the observational data are $d(t) = u_{\theta^*}(t) + \eta(t)$, where $u_{\theta^*}(t)$ comes from the solution of (1) and $\eta(t)$ is a correlated noise that evolves in time as

$$\eta(t_i) := \rho \eta(t_{i-1}) + \epsilon(t_i), \quad i = 2, \dots, N_t, \quad \eta(t_1) \sim \mathcal{N}\left(0, \frac{\sigma^2}{\Delta_t^2}\right) \quad (9)$$

with $|\rho| < 1$. The term $\epsilon(t_i)$ is independent from $\eta(t_{i-1})$ and the process ϵ is a normally distributed white noise. To reflect the model resolution Δ_t in the level of variance in noise η , we prescribe $\text{var}(\eta) = \sigma^2/\Delta_t^2$ together with ρ . The variance of η is constant across time since the process is stationary due to $|\rho| < 1$, meaning that the stationary distribution of the process is $\eta(t) \sim \mathcal{N}(0, \frac{\sigma^2}{\Delta_t^2})$ for all t . Consequently, we derive¹ $\epsilon(t_i) \sim \mathcal{N}(0, \frac{\sigma^2}{\Delta_t^2}(1 - \rho^2))$.

In the following, when noisy data are used, the values of the parameter ρ and σ are varied randomly across different samples of (2). We generate 100 independent samples of $\rho \sim \mathcal{N}(0.6, 0.05^2)$ and $\sigma \sim \mathcal{N}(0.07, 0.01^2)$ in order to achieve moderate correlation via ρ and a Δ_t -independent noise level of 5–10% For each value of the pair (ρ, σ) , independent replicates of the process η following (9) are generated and added to training and/or testing data.

Model parameter predictions with noise More relevant in practice are model parameter estimates in the presence of noise in observational data. Using a dense NN and a CNN, we demonstrate the effects of the additive noise stemming from the noise model described above on predictability.

¹Note that it is more common to prescribe $\text{var}(\epsilon)$ together with ρ first and then derive $\text{var}(\eta)$; however, we proceed in the reverse order because we are foremost interested in defining the effective variance of η .

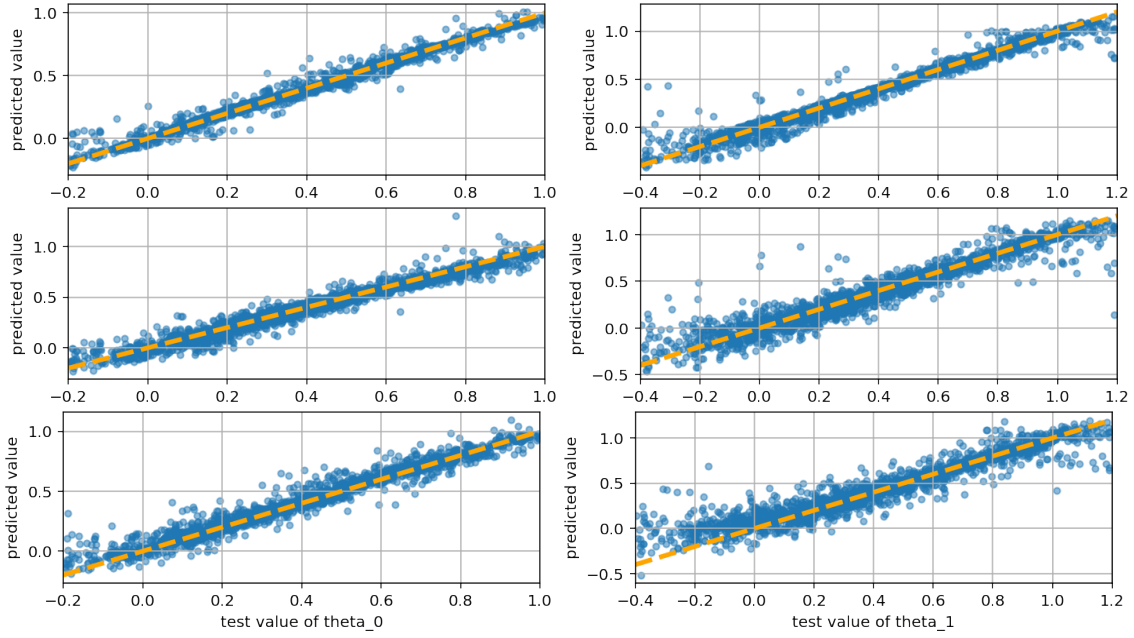


Figure 2: Predictions of parameters θ_0 (left column) and θ_1 (right column) from noise-free and noisy observational data, using a **dense NN** (4 layers, $n_u = 32$) and $N = 1000$ training samples. Top row: training and test data noise-free; Middle row: training data noise-free and test data with noise; Bottom row: training and test data with noise. Dashed orange line depicts perfect predictions.

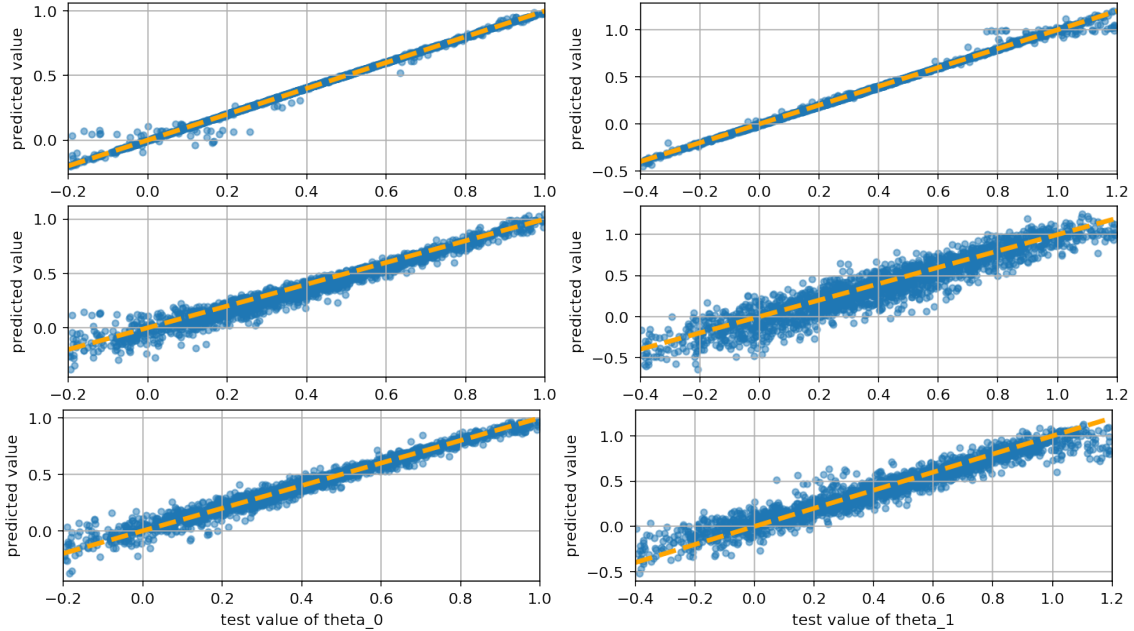


Figure 3: Predictions of parameters θ_0 (left column) and θ_1 (right column) from noise-free and noisy observational data, using a **CNN** ($n_f \times [1, 2, 4]$, $n_f = 8$) and $N = 1000$ training samples. Top row: training and test data noise-free; Middle row: training data noise-free and test data with noise; Bottom row: training and test data with noise. Dashed orange line depicts perfect predictions.

For these experiments, we choose the network architectures with the best prediction properties, given in Section 3.2, namely, a dense NN of four layers with 32 units per layer. For the CNN, we choose 3 convolutional layers with 8,16, and 32 filters in layers 1,2, and 3, respectively, followed by two dense layers with 32 units in each layer (denoted by $n_f \times [1, 2, 4]$ with $n_f = 8$ in Section 3.2). Tables 7 and 8 show the prediction errors for the dense NN and CNN, respectively. Three columns in each table represent different noise configurations: both training and testing data do not contain noise (second column); only testing data contain noise (third column); and both training and testing data contain noise (fourth column). The tables additionally demonstrate the effects of using smaller and larger amounts of training data, denoted by N (first column), indicating in most cases improved predictive skills with increasing training sets. Throughout all experiments, the testing data of size $M = 2000$ are kept fixed to allow for fair comparisons, and noise is added to the time series component of the testing data in certain experiment configurations.

For both networks, Tables 7 and 8 show the lowest prediction errors for noise-free training and testing data, whereas the highest prediction errors occur when the training data do not contain noise but the test data do have noise. For CNNs, predictions with noise in testing data improve if the training data are also noisy. These results show the importance of training CNNs with noisy data in practice, even if noise-free simulated model outputs are available, because data from experiments or measurements are very likely polluted by some amount of noise. Comparing the two network architectures, dense NN and CNN, the CNN delivers lower prediction errors in most cases except when the training of the CNN is performed with noise-free data while testing data have noise. Only in this case, the dense NN demonstrates significantly better predictability (R^2 of > 0.92 for dense NN vs. < 0.90 for CNN) and therefore shows that it is less sensitive to the presence or absence of noise in the training data.

We complete the discussion about prediction errors in the presence of observational noise by presenting scatter plots in Figures 2 and 3 describing the distribution of errors for varying values of model parameters θ_0 and θ_1 . Each graph in the figures shows the true value of θ_0 or θ_1 from the test data set on the horizontal axis and the corresponding predicted value on the vertical axis. Deviations of the predictions (blue dots) from the ideal (orange line) show the errors in predictability. The figures support the summarized statistics in Tables 7 and 8 discussed above and additionally show that the spread of prediction errors is largely uniform across values of θ_0 and θ_1 . Slightly larger errors can appear at the lower and upper bounds (5); these are more pronounced for the dense NN than for the CNN.

3.4 Simulations of FitzHugh–Nagumo model from predicted parameters

We extend the evaluation of results on model parameter predictions from the preceding Section 3.3 and now evaluate simulations of the FitzHugh–Nagumo model (1) with predicted parameters. The results in this section show the sensitivity of the predictions with respect to outputs of the forward problem. This section focuses on the CNN architecture with 3 convolutional layers and $n_f \times [1, 2, 4]$ filters, where $n_f = 8$, and we consider the three different cases of presence or absence of noise as in Section 3.3. Figure 4 represents the case where both training and testing data do not contain noise; in Figure 5 only testing data contain noise; and Figure 6 shows results where both training and testing data contain noise. Each figure contains several graphs where each graph is generated by using parameters achieving a given quantile of MSE values, in order to show the effects of a range of prediction accuracies on the FitzHugh–Nagumo model solutions.

We observe a nearly optimal overlapping of simulated output and test data for the noise-free case in Figure 4, even for the 75th percentile of MSE. When noise is added to training or testing data (Figures 5 and 6), the simulated time series for the median and higher percentiles show shifted

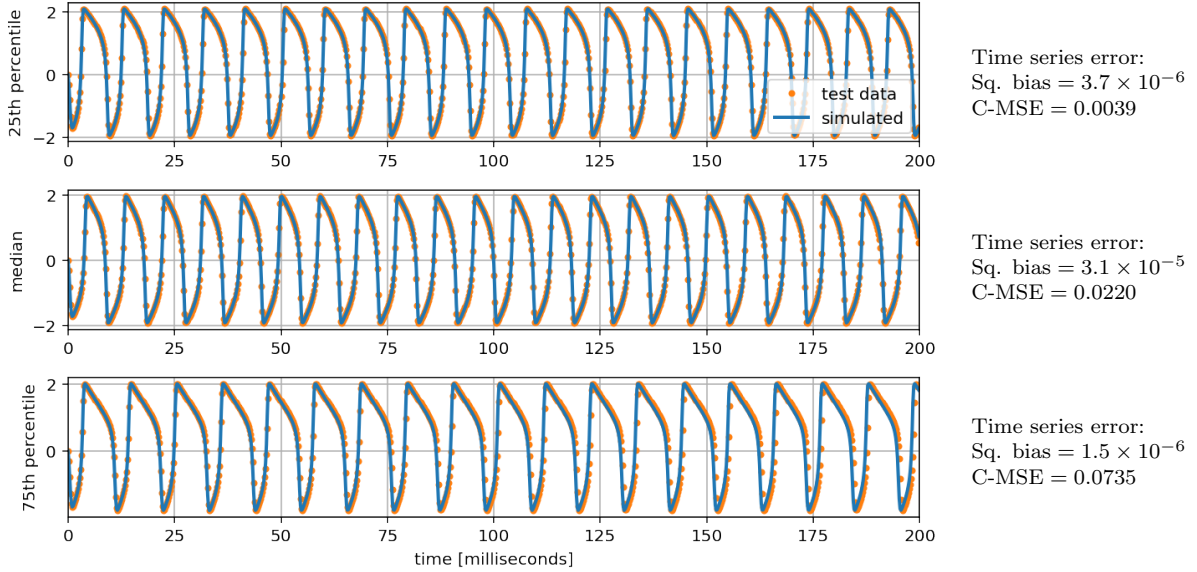


Figure 4: Simulations of FitzHugh–Nagumo model (blue lines) using parameters from **CNN** predictions; corresponding data that gave rise to prediction are shown as orange dots. Training samples ($N = 1000$) and test data ($M = 2000$) are both noise-free. Graphs from top to bottom show increasing quantiles of MSE between true and estimated parameters.

spikes, which become more pronounced as simulation time increases (100–200 milliseconds). The shifting of spikes over time represents discrepancies with respect to the frequency of a periodic time series. Overall, these results quantify the reliability of the proposed estimation in order to generate realistic solutions of the FitzHugh–Nagumo model from estimated parameters with CNN.

4 Conclusion

In this paper, we build an estimation framework for an inverse problem governed by an ODE, the FitzHugh–Nagumo model. The estimation consists of recovering model parameters as a prediction output from neural networks that are trained on time series solutions of the model as input. Our study shows the efficacy of neural network-based parameter recovery when traditional optimization techniques would fail to minimize the misfit function of the problem. In particular, we propose and compare a range of different architectures of dense and convolutional NNs in order to computationally learn reconstruction maps of the inverse problem in different situations (ideal train and test data, noisy train and test data, and noisy test data only). Prediction quality is carefully assessed through different statistical evaluation metrics and through the assessment of the FitzHugh–Nagumo model solutions calculated for the predicted model parameters. CNN architectures mostly show the lowest errors of recovered parameters, which can be attributed to their locally acting kernels being advantageous for time-evolving data. Additionally, the solutions of the ODE from these estimated parameters show accurate behaviors reinforcing the reliability of the proposed estimation framework for inverse problems. In only one case can dense networks achieve better results than CNNs, which is when training is performed with noise-free data whereas prediction data are polluted with noise. Thus, dense NNs demonstrate better generalization properties to test data with “unseen” noise levels.

Future directions include embedding uncertainty quantification methods in the NN-based pa-

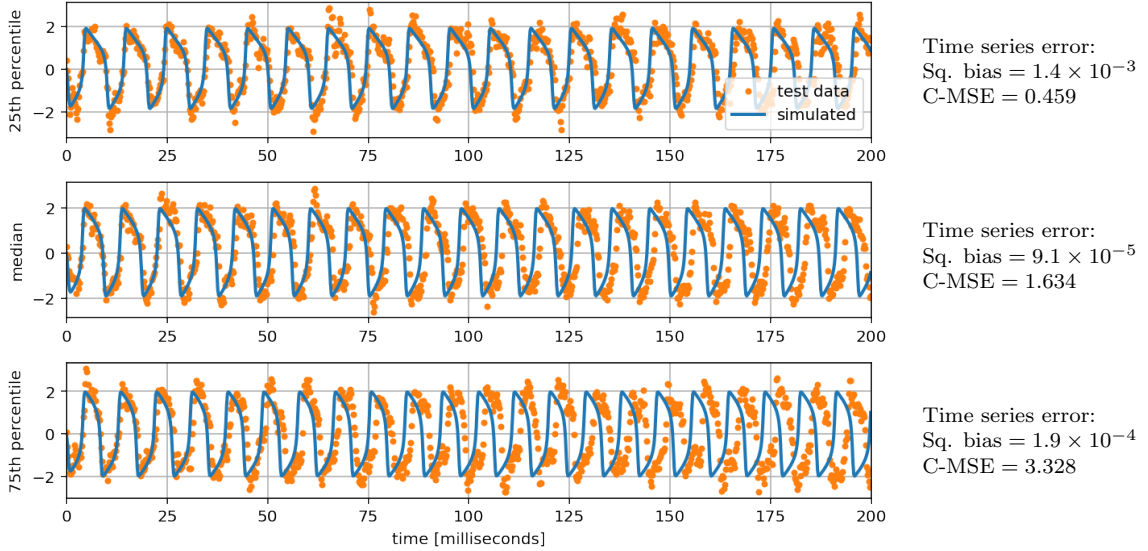


Figure 5: Simulations of FitzHugh–Nagumo model (blue lines) using parameters from **CNN** predictions. Training samples ($N = 1000$) are noise-free and test data ($M = 2000$) contains noise. Graphs from top to bottom show increasing quantiles of MSE between true and estimated parameters.

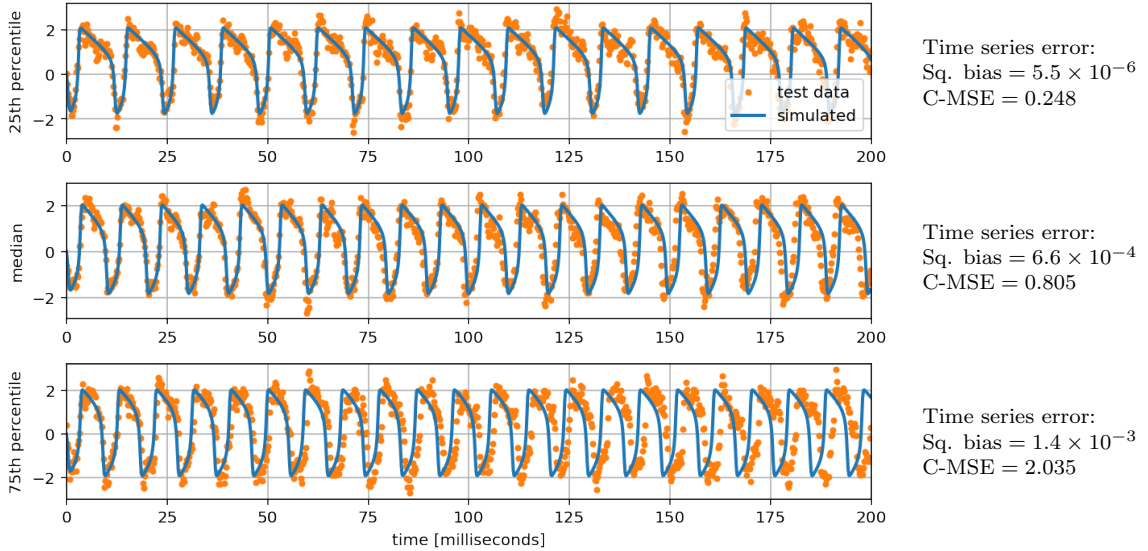


Figure 6: Simulations of FitzHugh–Nagumo model (blue lines) using parameters from **CNN** predictions. Training samples ($N = 1000$) and test data ($M = 2000$) both contain noise. Graphs from top to bottom show increasing quantiles of MSE between true and estimated parameters.

rameter estimations. Uncertainty can be considered with respect to model and data discrepancies but also with respect to network architecture and trained NN parameters. Some recent studies focus on loss functions and propose statistical losses that incorporate additional information about the data, such as the correlation structure of the observations and model outputs [8]. A different approach is to propose NN architectures for automatically selecting loss functions. [2] shows that loss functions for temporal statistical processes computed from a NN can effectively be used for inferring parameters within an ABC framework. The present work makes use only of the mean squared error as a loss; therefore, one can explore the incorporation of prior information and a description of uncertainty in order to approximate posteriors of the inverse problem. Our fitted reconstruction maps rely on training data that have to be generated by solving the forward problem numerous times. To mitigate the computational cost of training data generation, one can explore reduced order model techniques, which recently have been advanced through machine learning methods [39, 35].

Acknowledgments

The effort of Johann Rudi is based in part upon work supported by the U.S. Department of Energy, Office of Science, under contract DE-AC02-06CH11357. The effort of Amanda Lenzi and Julie Bessac is based in part on work supported by the U.S. Department of Energy, Office of Science, Office of Advanced Scientific Computing Research (ASCR), under contract DE-AC02-06CH11347.

References

- [1] Jonas Adler and Ozan Öktem. Solving ill-posed inverse problems using iterative deep neural networks. *Inverse Problems*, 33(12):124007, 2017. doi: 10.1088/1361-6420/aa9581.
- [2] Mattias Åkesson, Prashant Singh, Fredrik Wrede, and Andreas Hellander. Convolutional neural networks as summary statistics for approximate Bayesian computation. *arXiv preprint arXiv:2001.11760*, 2020.
- [3] Leandro M Alonso and Eve Marder. Visualization of currents in neural models with similar behavior and different conductance densities. *eLife*, 8:e42722, 2019. doi: 10.7554/eLife.42722.
- [4] Andrea Arnold and Alun L Lloyd. An approach to periodic, time-varying parameter estimation using nonlinear filtering. *Inverse Problems*, 34(10):105005, 2018. doi: 10.1088/1361-6420/aad3e0.
- [5] Benjamin Ballnus, Sabine Hug, Kathrin Hatz, Linus Görlitz, Jan Hasenauer, and Fabian J Theis. Comprehensive benchmarking of Markov chain Monte Carlo methods for dynamical systems. *BMC Systems Biology*, 11(64), 2017. doi: 10.1186/s12918-017-0433-1.
- [6] Laure Buhry, Sylvain Saighi, Audrey Giremus, Eric Grivel, and Sylvie Renaud. Parameter estimation of the Hodgkin–Huxley model using metaheuristics: application to neuromimetic analog integrated circuits. In *2008 IEEE Biomedical Circuits and Systems Conference*, pages 173–176. IEEE, 2008. doi: 10.1109/BIOCAS.2008.4696902.
- [7] Ki H Chon and Richard J Cohen. Linear and nonlinear ARMA model parameter estimation using an artificial neural network. *IEEE transactions on biomedical engineering*, 44(3):168–174, 1997.

- [8] Emil M Constantinescu, Noémi Petra, Julie Bessac, and Cosmin G Petra. Statistical treatment of inverse problems constrained by differential equations-based models with stochastic terms. *SIAM/ASA Journal on Uncertainty Quantification*, 8(1):170–197, 2020.
- [9] Kyle Cranmer, Johann Brehmer, and Gilles Louppe. The frontier of simulation-based inference. *Proceedings of the National Academy of Sciences*, 117(48):30055–30062, 2020. doi: 10.1073/pnas.1912789117.
- [10] Michael Creel. Neural nets for indirect inference. *Econometrics and Statistics*, 2:36–49, 2017.
- [11] Aidan C Daly, David J Gavaghan, Chris Holmes, and Jonathan Cooper. Hodgkin–Huxley revisited: reparametrization and identifiability analysis of the classic action potential model with approximate Bayesian methods. *Royal Society open science*, 2(12):150499, 2015. doi: 10.1098/rsos.150499.
- [12] Aidan C Daly, David Gavaghan, Jonathan Cooper, and Simon Tavener. Inference-based assessment of parameter identifiability in nonlinear biological models. *Journal of The Royal Society Interface*, 15(144):20180318, 2018. doi: 10.1098/rsif.2018.0318.
- [13] Bin Deng, Jiang Wang, and Yenqiu Che. A combined method to estimate parameters of neuron from a heavily noise-corrupted time series of active potential. *Chaos: An Interdisciplinary Journal of Nonlinear Science*, 19(1):015105, 2009. doi: 10.1063/1.3092907.
- [14] Shinji Doi, Yuichi Onoda, and Sadatoshi Kumagai. Parameter estimation of various Hodgkin–Huxley-type neuronal models using a gradient-descent learning method. In *Proceedings of the 41st SICE Annual Conference. SICE 2002.*, volume 3, pages 1685–1688. IEEE, 2002. doi: 10.1109/SICE.2002.1196569.
- [15] Resat Ozgur Doruk and Laila Abosharb. Estimating the parameters of FitzHugh–Nagumo neurons from neural spiking data. *Brain Sciences*, 9(12):364, 2019. doi: 10.3390/brainsci9120364.
- [16] Vivek Dua. An artificial neural network approximation based decomposition approach for parameter estimation of system of ordinary differential equations. *Computers & chemical engineering*, 35(3):545–553, 2011.
- [17] Stefan Elfwing, Eiji Uchibe, and Kenji Doya. Sigmoid-weighted linear units for neural network function approximation in reinforcement learning. *Neural Networks*, 107:3–11, 2018. doi: 10.1016/j.neunet.2017.12.012.
- [18] Richard FitzHugh. Impulses and physiological states in theoretical models of nerve membrane. *Biophysical Journal*, 1(6):445–466, 1961.
- [19] Pedro J Gonçalves, Jan-Matthis Lueckmann, Michael Deistler, Marcel Nonnenmacher, Kaan Öcal, Giacomo Bassetto, Chaitanya Chintaluri, William F Podlaski, Sara A Haddad, Tim P Vogels, David S Greenberg, and Jakob H Macke. Training deep neural density estimators to identify mechanistic models of neural dynamics. *eLife*, 9:e56261, 2020. doi: 10.7554/eLife.56261.
- [20] Ian Goodfellow, Yoshua Bengio, and Aaron Courville. *Deep Learning*. MIT Press, 2016.
- [21] Ryan N Gutenkunst, Joshua J Waterfall, Fergal P Casey, Kevin S Brown, Christopher R Myers, and James P Sethna. Universally sloppy parameter sensitivities in systems biology models. *PLOS Computational Biology*, 3(10):e189, 2007. doi: 10.1371/journal.pcbi.0030189.

- [22] Franz Hamilton, Tyrus Berry, and Timothy Sauer. Tracking intracellular dynamics through extracellular measurements. *PLoS one*, 13(10):e0205031, 2018. doi: 10.1371/journal.pone.0205031.
- [23] Soufiane Hayou, Arnaud Doucet, and Judith Rousseau. On the selection of initialization and activation function for deep neural networks. *arXiv preprint arXiv:1805.08266*, 2018.
- [24] Alan L Hodgkin and Andrew F Huxley. A quantitative description of membrane current and its application to conduction and excitation in nerve. *The Journal of physiology*, 117(4):500–544, 1952.
- [25] Bai Jiang, Tung-yu Wu, Charles Zheng, and Wing H. Wong. Learning summary statistic for approximate Bayesian computation via deep neural network. *Statistica Sinica*, pages 1595–1618, 2017.
- [26] Renaud Jolivet, Alexander Rauch, Hans-Rudolf Lüscher, and Wulfram Gerstner. Predicting spike timing of neocortical pyramidal neurons by simple threshold models. *Journal of Computational Neuroscience*, 21(1):35–49, 2006. doi: 10.1007/s10827-006-7074-5.
- [27] Jari Kaipio and Erkki Somersalo. *Statistical and Computational Inverse Problems*, volume 160 of *Applied Mathematical Sciences*. Springer-Verlag New York, 2005. doi: 10.1007/b138659.
- [28] Diederik P Kingma and Jimmy Ba. Adam: A method for stochastic optimization. In *International Conference for Learning Representation*, 2015.
- [29] Alex Krizhevsky, Ilya Sutskever, and Geoffrey E Hinton. ImageNet classification with deep convolutional neural networks. In *Advances in Neural Information Processing Systems*, volume 25, pages 1097–1105. Curran Associates, Inc., 2012.
- [30] Yann LeCun, Patrick Haffner, Léon Bottou, and Yoshua Bengio. Object recognition with gradient-based learning. In *Shape, contour and grouping in computer vision*, pages 319–345. Springer, 1999.
- [31] Terence C Mills. *Time Series Techniques for Economists*. Cambridge University Press, 1991.
- [32] Jahangir Morshed and Jagath J. Kaluarachchi. Parameter estimation using artificial neural network and genetic algorithm for free-product migration and recovery. *Water Resources Research*, 34(5):1101–1113, 1998.
- [33] Jinichi Nagumo, Suguru Arimoto, and Shuji Yoshizawa. An active pulse transmission line simulating nerve axon. *Proceedings of the IRE*, 50(10):2061–2070, 1962.
- [34] Richard Naud, Brice Bathellier, and Wulfram Gerstner. Spike-timing prediction in cortical neurons with active dendrites. *Frontiers in Computational Neuroscience*, 8:90, 2014. doi: 10.3389/fncom.2014.00090.
- [35] Thomas O’Leary-Roseberry, Umberto Villa, Peng Chen, and Omar Ghattas. Derivative-informed projected neural networks for high-dimensional parametric maps governed by PDEs. *arXiv preprint arXiv:2011.15110*, 2020.
- [36] Stefano Pagani, Andrea Manzoni, and Alfio Quarteroni. Efficient state/parameter estimation in nonlinear unsteady PDEs by a reduced basis ensemble Kalman filter. *SIAM/ASA Journal on Uncertainty Quantification*, 5(1):890–921, 2017. doi: 10.1137/16M1078598.

- [37] Jaimit Parikh, James Kozloski, and Viatcheslav Gurev. Integration of AI and mechanistic modeling in generative adversarial networks for stochastic inverse problems. *arXiv preprint arXiv:2009.08267*, 2020.
- [38] Astrid A Prinz, Dirk Bucher, and Eve Marder. Similar network activity from disparate circuit parameters. *Nature Neuroscience*, 7(12):1345–1352, 2004. doi: 0.1038/nn1352.
- [39] Elizabeth Qian, Boris Kramer, Benjamin Peherstorfer, and Karen Willcox. Lift & learn: Physics-informed machine learning for large-scale nonlinear dynamical systems. *Physica D: Nonlinear Phenomena*, 406:132401, 2020. doi: <https://doi.org/10.1016/j.physd.2020.132401>.
- [40] Stefan T. Radev, Ulf K. Mertens, Andreass Voss, Lynton Ardizzone, and Ullrich Köthe. BayesFlow: Learning complex stochastic models with invertible neural networks. *arXiv preprint arXiv:2003.06281*, 2020.
- [41] Jürgen Schmidhuber. Deep learning in neural networks: An overview. *Neural networks*, 61: 85–117, 2015.
- [42] Albert Tarantola. *Inverse Problem Theory and Methods for Model Parameter Estimation*. SIAM, Philadelphia, PA, 2005.
- [43] Karl E Taylor. Summarizing multiple aspects of model performance in a single diagram. *Journal of Geophysical Research: Atmospheres*, 106(D7):7183–7192, 2001.
- [44] Werner Van Geit, Erik De Schutter, and Pablo Achard. Automated neuron model optimization techniques: a review. *Biological Cybernetics*, 99:241–251, 2008. doi: 10.1007/s00422-008-0257-6.

Government License: The submitted manuscript has been created by UChicago Argonne, LLC, Operator of Argonne National Laboratory (“Argonne”). Argonne, a U.S. Department of Energy Office of Science laboratory, is operated under Contract No. DE-AC02-06CH11347. The U.S. Government retains for itself, and others acting on its behalf, a paid-up nonexclusive, irrevocable worldwide license in said article to reproduce, prepare derivative works, distribute copies to the public, and perform publicly and display publicly, by or on behalf of the Government. The Department of Energy will provide public access to these results of federally sponsored research in accordance with the DOE Public Access Plan. <http://energy.gov/downloads/doe-public-access-plan>